Formation of Two Homologous Transequatorial Loops

Jie Chen[1,2] · Alexei A. Pevtsov[3] · Jiangtao Su[1,4] ·
Robertus Erdélyi[2,5] · Yuanyong Deng[1] ·
Shangbin Yang[1] · Yongliang Song[1]

Abstract The formation mechanism of two homologous transequatorial loops (TLs) of July 7–8, 1999 (SOL1999-07-07) is studied. The TLs connected active region AR 8614 from the northern hemisphere to AR 8626 in the southern hemisphere. The first TL appeared as a distinct structure at 12:49 UT on July 7, the second TL appeared at 06:21 UT, on July 8. Important results are obtained in this analysis: (i) The configuration of the two TLs is similar in X-rays. (ii) The sizes of the two active regions related to the TLs increased before and during the formation of the two TLs, this induced the expansion of their coronal loops. (iii) Both TLs formed globally on a time scale shorter than 110 min (time resolution of observations). (iv) An X-shaped coronal structure was observed. This observational evidence suggests that the two TLs formed by the same physical mechanism, magnetic reconnection, between the two expanding magnetic configurations of the two ARs.

Keywords Solar activity · Coronal loops · Magnetic fields · Magnetic reconnection · Chromospheric evaporation

✉ J. Chen
  chenjie@bao.ac.cn

1   Key Laboratory of Solar Activity, National Astronomical Observatories, Chinese Academy of Science, Beijing 100101, China

2   Solar Physics and Space Plasma Research Centre (SP2RC), School of Mathematics and Statistics, University of Sheffield, Sheffield, UK

3   National Solar Observatory, Boulder, CO 80303, USA

4   School of Astronomy and Space Sciences, University of Chinese Academy of Sciences, 19A Yuquan Road, Beijing 100049, China

5   Department of Astronomy, Eötvös Loránd University, Budapest, Hungary

1. Introduction

Transequatorial loops (TLs) are large-scale bright structures whose footpoints are rooted in different regions in opposite hemispheres. The first observation of TL was obtained by Skylab in the 1970s (e.g. Švestka *et al.*, 1977). Next, the Yohkoh satellite was launched in 1991, and the Soft X-ray Telescope (SXT) on-board the Yohkoh satellite detected a large number of soft X-ray images in more than 10 years of observation. Several hundreds of TLs were identified (Pevtsov, 2000; Chen, Bao, and Zhang, 2006, 2007).

Through a statistical study, Chen, Bao, and Zhang (2006) found that about 66% of TLs connect the preceding polarity among more than three hundreds TLs, and this preference is independent of solar cycle. The number of TLs varies in accordance with the sunspot number during the solar cycle. The separation of TLs, that is, the distance between the two footpoints of TLs, follows a trend as part of the solar cycle: at the beginning of a solar cycle, the separation has a maximum value; then, following the evolution of the solar cycle, the value of separation decreases. Pevtsov (2000) found that 68% of cases had the same chirality in 22 pairs of active regions connected by TLs. Chen, Bao, and Zhang (2007) investigated 43 pairs of active regions connected by TLs and found that a little more than 50% of active regions have the same chirality. They also found that the twist pattern of TLs tends to be the same as the related active regions. As two footpoints of the same magnetic flux tube must have the same helicity (twist), one may wonder how to interpret the above observation. As an option, the transequatorial loops could connect patches of the same helicity, which are known to exist inside sunspots (e.g., Pevtsov, Canfield, and Metcalf, 1994).

The evolution of TLs may be related to flares and coronal mass ejections (CME). Khan and Hudson (2000) found that flare-generated shock waves may cause the eruption of TLs and then the disappearance of TL triggered CME. TL is one type of large-scale magnetic sources of CMEs (Zhou, Wang, and Zhang, 2006, Zhang *et al.*, 2007). Wang *et al.* (2007) found that the brightness of TL has a relation with the initiation of a halo-CME. Moon (2002) found that sympathetic flares are more favorably produced in active region pairs with TLs. Chen, Lundstedt, and Zhang (2010) showed, through a statistical study, that the twist value of the TLs has a weak relation with the flare flux.

Magnetic reconnection is considered to play an important role in the formation of TLs. Tsuneta (1996) demonstrated that a TL was formed in X-type reconnection. Later, Fárnik, Karlicky, and Svestka (1999) observed that TLs originate from two active regions nearby the solar equator through magnetic reconnection and suggested that reconnection is caused by the difference in the rotation rate of the two regions. While the term "loops" has been broadly applied to TL-structures, Pevtsov (2004) argued that some of TLs could be magnetic separators, not loops. His arguments were based on the shape of these structures and on scaling laws between the structure's length and its brightness. Yokoyama and Masuda (2009, 2010) analyzed a TL generated through magnetic reconnection between weak magnetic fields of coronal holes and strong magnetic fields of active regions. Balasubramaniam *et al.* (2011) described an example of change in large-scale connectivity associated with the emergence of a small active region. New connections, which developed between new and mature active regions, affected the connectivity in other part of corona, and eventually led to a filament eruption. Recently, Du *et al.* (2018) analyzed the formation of large-scale coronal interconnecting loops with high resolution data. The detailed formation process of TL is not yet well-understood. Based on these previous studies, the nature of TLs remains unclear.

In this paper, we report on two homologous TLs that occurred during July 7 to 8, 1999. The formation processes are described and the related photospheric magnetic field is analyzed. In Section 2, we introduce the instrument, data reduction and method. The detailed

observations and results are demonstrated in Section 3. In Section 4, we make a summary of observations. In the last section, we present our conclusions and discussion.

2. Instrument and Data Reduction

2.1. SXT

While transequatorial loops can be seen in EUV and X-ray (narrow-band) bandpasses, they are better visible in broad-band soft X-ray data, such as that of the Soft X-ray Telescope (SXT) flown on-board the Yohkoh satellite. The majority of investigations of TLs were made using SXT. The Yohkoh satellite was launched in 1991 and observed the solar atmosphere in X-ray radiation for about ten years. The SXT (Tsuneta, 1991) was a grazing-incidence reflection telescope with a CCD detector (1024×1024). It provided both full- and partial-disk images which cover the whole Sun or only a local region of interest. In this study, we use the full-disk soft X-ray images with spatial resolution of 4.9″ per pixel. The images were taken using the Al.1 and AlMg filters. Data are downloaded from http://solar.physics.montana.edu/ylegacy/. The corrected and composite level-2 data, which were taken using the AlMg filter are selected, because they seem to show TLs better than other wavelength bands.

The data obtained from SXT without regular temporal resolution, we selected all the available data obtained by AlMg filter with 512×512 pixel.

The temperature is estimated using the data obtained by Al.1 and AlMg filters. The routine sxt_teem.pro is used to estimate the temperature with the filter-ratio method.

2.2. MDI

SOHO Michelson and Doppler Instrument (MDI) instrument (Scherrer *et al.*, 1995) measured the magnetic signal by differencing Dopplergrams obtained in right- and left-circular polarized light. The observation of MDI consists of full-disk line-of-sight (LOS) magnetograms taken with a time cadence of 96 minutes and a pixel size of 1.96″. The re-calibrated level 1.8.2 data are used. The new calibrated data employ an improved sensitivity flatfield map and pixels with obvious cosmic-ray contamination have been removed. The same method, as described in Chen *et al.* (2011), is used to deal with the LOS magnetograms including co-aligning the images, removing differential rotation effects, and making geometric correction.

2.3. Calculation of Accumulated Magnetic Helicity

Using MDI data, we investigate the changes in magnetic helicity associated with the formation of TLs. The change in the magnetic helicity H_R in an open volume can be expressed as

$$\frac{dH_R}{dt} = -2 \int \left((\boldsymbol{A}_P \cdot \boldsymbol{V})\boldsymbol{B} - (\boldsymbol{A}_p \cdot \boldsymbol{B})\boldsymbol{V} \right) \cdot d\boldsymbol{S}. \tag{1}$$

The first term of Equation 1 represents the effect of shearing motion of the boundary, and the second term represents the bulk transport of the helical field across the boundary. A more detailed description for the above equation can be found in e.g. Berger (1999). The transport rate of magnetic helicity from the sub-photosphere to corona by the photospheric horizontal motions is described by the equation

$$\frac{dH_R}{dt} = -2 \int (\boldsymbol{A}_p \cdot \boldsymbol{U}) B_n d\boldsymbol{S}, \tag{2}$$
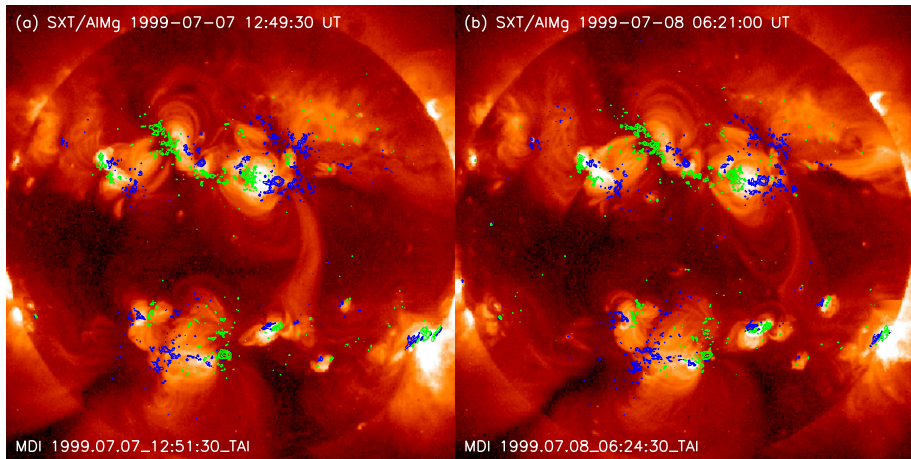
Figure 1 Two TLs observed by Yohkoh/SXT on July 7 (a) and 8 (b), 1999. The line-of-sight (LOS) magnetic fields of MDI are superimposed on the two panels, where the blue/green contours denote positive/negative magnetic field.

which was originally derived by Démoulin and Berger (2003), where U is the horizontal velocity and B_n is the normal component of the photospheric magnetic field. This method is commonly applied to MDI data (see, e.g. Liu and Zhang, 2006; Yang *et al.*, 2009).

The accumulated magnetic helicity during time t can be expressed as

$$H(t) = \int_0^t \frac{dH_R(t)}{dt} dt, \tag{3}$$

where t = 0 corresponds to the starting moment of calculation.

3. Observation and Results

Two homologous TLs developed on July 7-8, 1999 connected AR 8614 located in the northern hemisphere and AR 8626 in the southern hemisphere (Figure 1). In order to describe the two TLs more conveniently, we name the TL in Figure 1a as "TL1", and the TL in Figure 1b as "TL2". The evolution processes of the successive TLs are shown in Movie 1. AR 8614 appeared on the east edge of the Sun on 1999 July 2 and it developed into a complex active region with $\beta\gamma$ magnetic type on July 6 (Figure 2b). AR 8626 is a new-born active region showing a rapid magnetic flux emergence from July 6. It developed into a $\beta\gamma$-type active region on July 8 (Figure 2c). The evolution of magnetic flux in the two active regions was studied by Chen *et al.* (2011).

3.1. Evolution of AR 8614

AR 8614 was located at N19W21, and it was a $\beta\gamma$-type active region on July 7, 1999. From July 5 to July 8, the variation of the size of the active region, the distance between the barycenter of positive magnetic flux (PMGC) and the one of negative magnetic flux
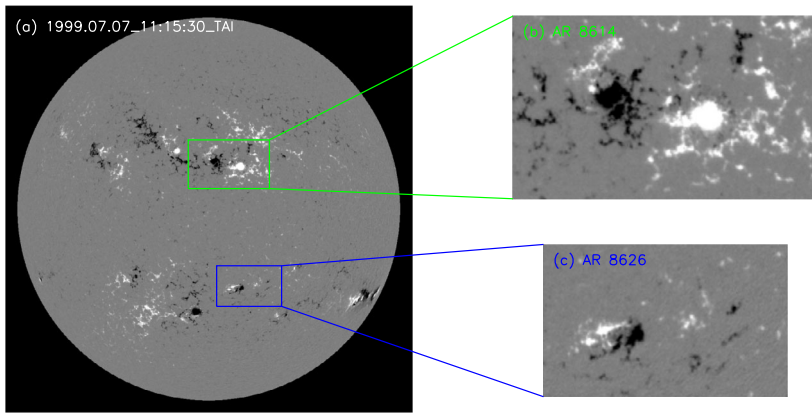
Figure 2 (a) A full-disk LOS magnetogram of MDI on July 7, 1999. The regions for ARs 8614 and 8626 are extracted from the full-disk magnetogram and shown in (b) and (c), respectively.

(NMGC) is calculated. First of all, we calculated the magnetic gravity center of each polarity using the following formula:

$$X_c = \frac{\sum X_i F_i}{\sum F_i}, \ Y_c = \frac{\sum Y_j F_j}{\sum F_j}. \tag{4}$$

Here F(i, j) indicates the measured longitudinal magnetic field intensity. Then we determined the distance between PMGC and NMGC.

Figure 3 demonstrates how we calculate the distance, and the variation of the distance between PMGC and NMGC in AR 8614 from July 5, 8:00 UT to the end July 8. Figure 3a displays PMGC (the green cross), NMGC (the blue cross), and the distance between PMGC and NMGC (the red line) at 17:39 UT on July 5, Figure 3b displays the distance at 11:15 UT on July 7. Comparing the red line in Figure 3a and that of Figure 3b, the one in Figure 3b is clearly longer than its counterpart in Figure 3a. Next, Figure 3c shows that the distance variation between PMGC and NMGC from July 5, 8:00 UT to the end of July 8. At July 5, 8:00 UT, the distance is around 59 Mm, then it increased gradually, and at around 17:00 UT on July 7, the distance became the longest (around 82 Mm). From that time, there is almost no variation of the distance till the end of July 8. Figure 3c indicates that the size of AR 8614 mainly increased from July 5, 8:00 UT to July 7, 17:00 UT.

3.2. Evolution of AR 8626

AR 8626, a rapidly developing new-born AR in the southern hemisphere, which emerged on July 5, 1999. The evolution of AR 8626 in SXT is depicted in Figure 4. The coronal loops progressively transform into a sigmoidal configuration (Figure 4i). This forward-S shaped sigmoid structure indicates a positive twist (Rust and Kumar, 1996; Canfield, Hudson, and McKenzie, 1999). Figures 2c and 5 show that the emerging AR 8626 has magnetic tongues (Luoni *et al.*, 2011; Poisson *et al.*, 2016) that indicate the emergence of a flux rope with positive twist in agreement with the forward-S shape.

Figure 12 of Chen *et al.* (2011) shows the evolution of magnetic field of this active region. On July 6, the magnetic bipolar region was small, then magnetic flux emerged rapidly. More than a day later, at 6:27 UT on July 7, AR 8626 appeared with an obvious magnetic structure:
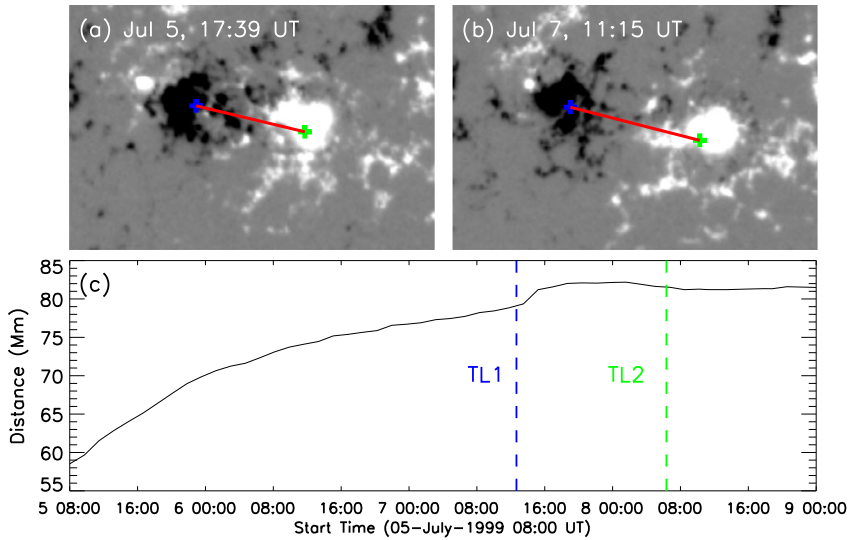
Figure 3 Variation of distance between the barycenters of positive and negative magnetic polarities of AR 8614. (a) An MDI LOS magnetogram observed at 17:39 UT on July 5. (b) An MDI magnetogram observed at 11:15 UT on July 7. Green cross marks the PMGC, blue cross marks the NMGC, the red line shows the distance between PMGC and NMGC, FOV: 297″ × 198″. (c) Distance vs. time from July 5, 08:00 UT to July 9, 00:00 UT. The blue and green dashed lines show the peak times of TL1 and TL2.

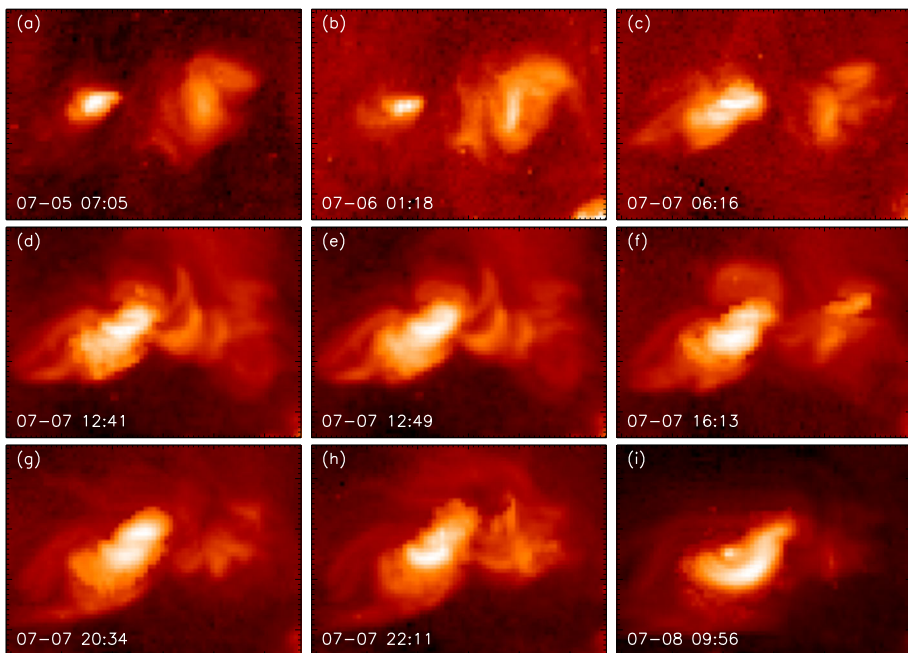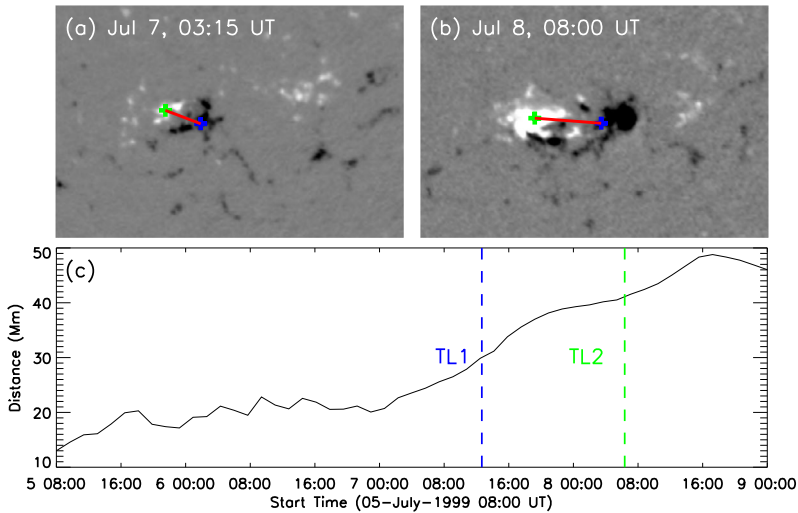**Figure 4** Evolution of AR 8626 observed by Yohkoh/SXT. The FOV is 343.7″ × 245.5″.

Figure 5 Same as Figure 3 but for AR 8626. (a) An MDI LOS magnetogram observed at 03:15 UT on July 7, FOV: $297'' \times 198''$. (b) An MDI magnetogram observed at 08:00 UT on July 8. (c) Distance vs. time from July 5, 08:00 UT to July 9, 00:00 UT. The blue and green dashed lines show the peak times of TL1 and TL2.

the preceding polarity is negative and the following polarity is positive. Figure 13 of Chen *et al.* (2011) shows that the magnetic flux increased up to 6×10^{21} Mx from the end of July 6 to the end of July 7.

The magnetic configuration and the variation of distance between PMGC and NMGC in AR 8626 are shown in Figure 5. In Figures 5a and 5b, the red lines show the distance between PMGC and NMGC of AR 8626 at 03:15 UT on July 7 and at 08:00 UT on July 8, respectively. Comparing the distance in Figure 5a and that of Figure 5b, the one in Figure 5b is obvious longer than its counterpart in Figure 5a. In order to have the same time interval as for AR 8614, the variation of distance between PMGC and NMGC of AR 8626 is also from July 5, 8:00 UT, to the end of July 8, which is plotted in Figure 5c. From Figure 5c, the distance from July 5, 8:00 UT to the end of July 6 is mostly constant. Figure 13d in the paper of Chen *et al.* (2011) also shows the total magnetic flux ($\Phi_{tot} = \sum \Phi_{pos} + |\sum \Phi_{neg}|$) has no obvious variation on July 6. That means AR 8626 just emerged without rapid development. In Figure 5c, from the beginning of July 7 to July 8, 16:00 UT, the distance began to increase rapidly with the length changing from ~ 20 Mm to ~ 50 Mm, which indicates that the increased distance is about 30 Mm in about two days.

3.3. Accumulation of Magnetic Helicity in Two Active Regions

The accumulated magnetic helicity of AR 8614 in the northern hemisphere and AR 8626 in the southern hemisphere are calculated. From Figure 6, we can see the accumulated magnetic helicity in AR 8614 is negative, and in AR 8626 it is positive. The hemispheric helicity rule exhibits that most active regions in the northern hemisphere are with negative helicity and those in the southern hemisphere with positive helicity (e.g. Pevtsov, Canfield, and Metcalf, 1995; Bao and Zhang, 1998; Xu *et al.*, 2009; Hao and Zhang, 2011). Both active regions (AR 8614 and AR 8626) are consistent with the hemispheric helicity rule.

Fárník, Karlicky, and Svestka (1999) found that two TLs originated through reconnection of field lines extending from two active regions with the same chirality. Pevtsov (2000),
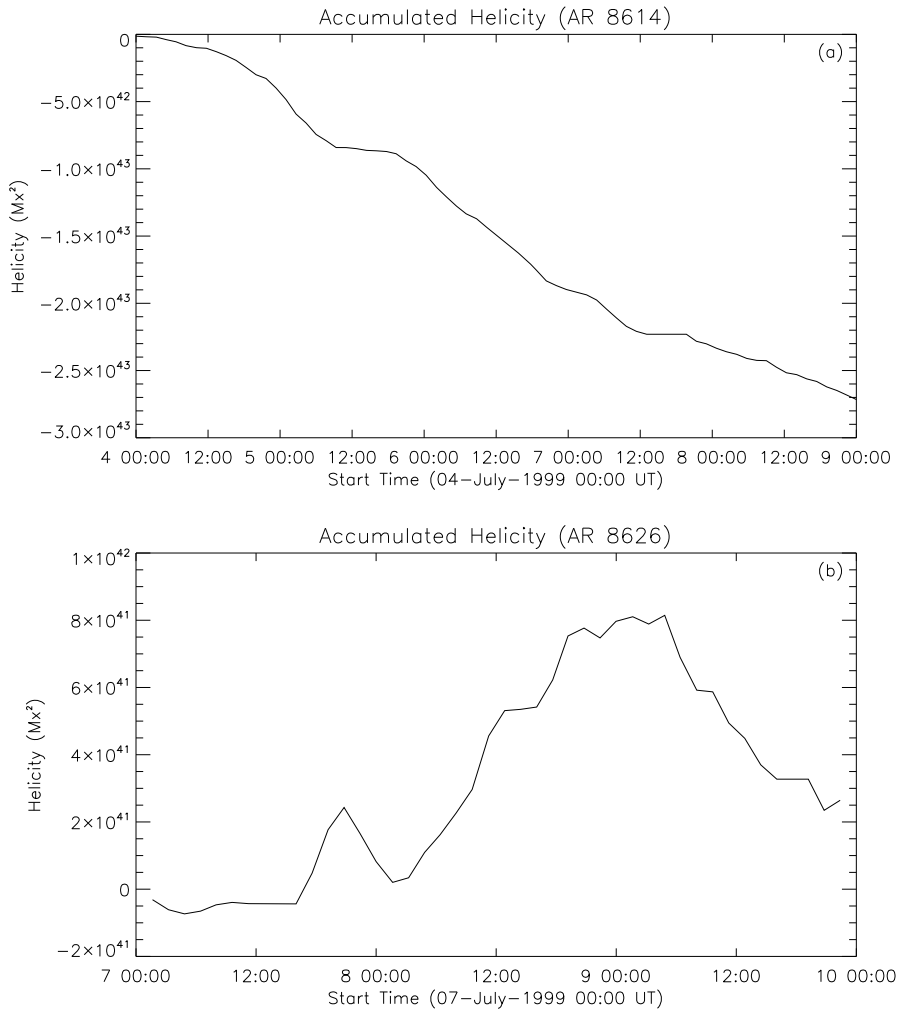
Figure 6 The accumulated magnetic helicity in two active regions. (a) in AR 8614 and (b) in AR 8626.

through a statistical study, found that in most cases transequatorial interconnecting regions have the same chirality. Later, Chen, Bao, and Zhang (2007) found that only in a little more than a half cases transequatorial interconnecting regions have the same chirality. For the present case, TL connected two active regions with opposite chirality rather than the same chirality.

3.4. Formation of TL1

The formation process of TL1 in soft X-ray images is demonstrated in Figure 7. Originally, at 01:18:40 UT on July 6, there was no clear brightness at the TL position (Figure 7a). More than a day later, at 06:16 UT on July 7, a narrow, bright TL appeared (Figure 7b) which connected the positive polarity in AR 8614 and negative polarity in AR 8626. At 10:46, we can see, there were perhaps two TLs (Figure 7c). After that, the TL became wider and
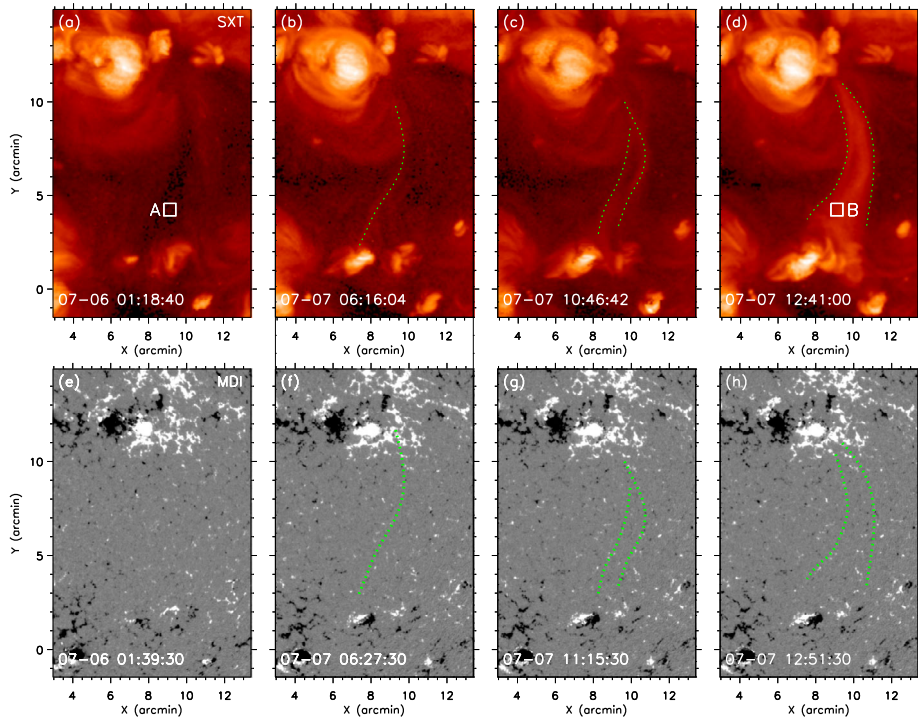
Figure 7 Top panel: Formation process of TL1 captured in soft X-rays. Reference time: 1999-07-07 12:41:00 UT. Bottom panel: the corresponding magnetograms obtained from SOHO/MDI. Green dotted lines demonstrate the morphology of TL1. The FOV of all panels is $10.46' \times 16.37'$.

brighter, till 12:41 UT, when the TL became the brightest (Figure 7d). The corresponding photospheric LOS magnetograms observed by MDI are shown in Figures 7e - 7h. The field of view (FOV) in the bottom panel is almost the same as the FOV in the top panel of Figure 7, and the observing time in the bottom panel is the closest to the observing time in the top panel of Figure 7.

We observe the TL structure first at 6:16, on July 7. Following the evolution of this TL, we observe that the coronal loops in AR 8614 became larger and larger. From the top panel of Figure 7, we can see that the coronal loops gradually extended towards the south direction.

From its first appearance (see, movie, frame July 7, 06:16:04 UT), this TL exhibits a somewhat complex structure. It is not a "single loop" but its southern end appears to have several "loops" rooted in magnetic polarities west of AR 8626. AR 8626 emerged behind another small bipolar region with a similar orientation (well visible at the bottom of Figure 7 and even more in Figure 12 of Chen *et al.*, 2011). This creates a quadrupole configuration with three types of connectivities which can be seen in SXT images (Figure 4). This magnetic configuration could induce that the southern end of this TL appeared as several "loops".

The filter-ratio method is used to estimate the temperature of the region before and after TL1 appearance. The average temperatures of the square box A (in Figure 7a) and B (in Figure 7d) are 0.25 MK and 3.35 MK, respectively. The temperature increases rapidly when the TL1 appears. This obvious difference in the temperatures indicate that there is a global heating during the formation of TL1.
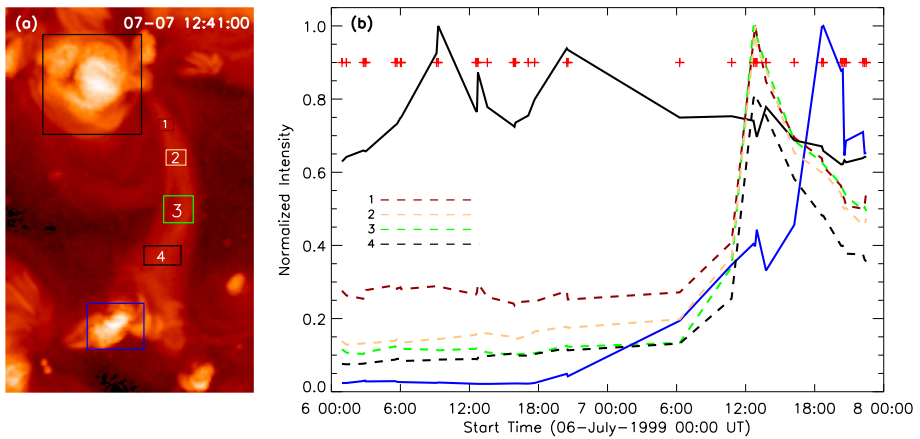
Figure 8 (a): An SXT image with TL1 observed at 12:41 UT on July 7, 1999. The black/blue box shows the selected region of AR 8614/AR 8626, respectively. Four segments of TL1 are marked by boxes with different colors and labeled by 1, ..., 4 on the image. (b) Normalized intensity variation of the four segments of TL1 and the related active regions from the beginning of July 6 to the end of July 7. The black/blue curve shows the normalized intensity variation of AR 8614/AR 8626, respectively. The four dashed curves show the normalized intensity variation of TL1 in different segments which are marked by boxes 1, ..., 4. The red crosses indicate the observing time of SXT images (the accurate time of the data are listed in Table 1).

Table 1 SXT observation time of TL1.

Date	Time	Date	Time	Date	Time	Date	Time
06	00:55:28	06	01:18:40	06	02:46:44	06	02:55:18
06	02:59:32	06	05:33:32	06	05:42:10	06	06:00:44
06	06:05:14	06	09:08:30	06	09:17:04	06	12:33:34
06	12:38:54	06	12:44:20	06	13:33:34	06	15:49:10
06	15:54:36	06	15:59:54	06	17:06:38	06	17:39:42
06	20:27:38	06	20:32:58	07	06:16:04	07	10:46:42
07	12:41:00	07	12:49:30	07	12:58:02	07	13:46:12
07	16:13:32	07	18:37:24	07	18:45:06	07	20:17:48
07	20:26:20	07	20:34:58	07	20:43:24	07	22:11:56
07	22:20:32	07	22:29:02				

3.5. Intensity Variation of TL1

The normalized intensity variation of the TL, in different segments, and the related two active regions from the beginning of July 6 to the end of July 7 are presented in Figure 8. The selected regions are marked in Figure 8a, where the temporal variations of the normalized intensity of the selected regions are plotted in Figure 8b. All the SXT data observed using the AlMg filter with 512×512 pixels are used in this analysis, and detailed information of these data are listed in Table 1. Their times are marked in Figure 8b with red.

The black/blue curves denote the intensity variation of the entire AR 8614/8626. At the beginning, its normalized value is around 0.6. Later, there are two peaks during July 6. Before 18:00 UT on July 6, the value is almost zero, after that, the intensity increased gradually.
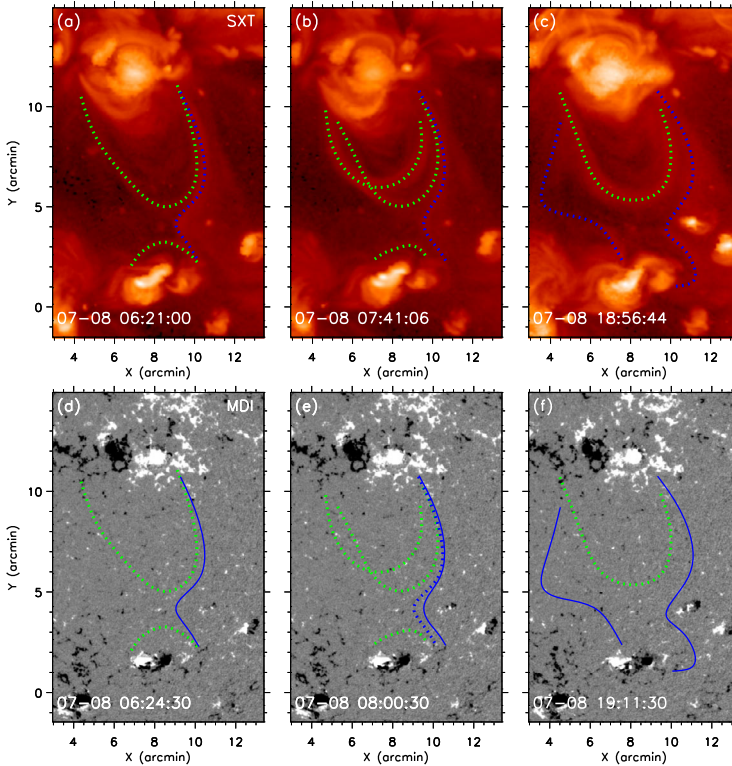
Figure 9 Same as Figure 7 but for TL2. Reference time: 1999-07-07 12:41:00 UT. In Figure 9e, the blue dotted line shows the TL observed at 06:21 UT, the blue continuous line show the TL observed at 07:41 UT.

Four segments are selected to monitor the intensity variation along TL1. The selected regions are marked by boxes with different colors and labeled with 1, 2, 3 and 4. The temporal evolution of the normalized intensity are plotted with four different dashed curves in Figure 8b. The four dashed curves have the same tendency: around 06:10 UT on July 7, they began to increase, after that they increased quickly, at around 12:41 UT, the intensity arrived at its peak value, and later, they decreased simultaneously.

From Figure 8b, we can see that the variations of the normalized intensity of TL1 are simultaneous in different segments. The increase of normalized intensity of TL1 is following the increase of normalized intensity in AR 8626. The variation of normalized intensity of TL1 has no relation with the variation of normalized intensity in AR 8614.

3.6. Formation of TL2

The morphology and evolution of TL2 are visualized in Figure 9. The large-scale loops in active regions are outlined with green dotted lines. TLs are outlined with blue lines. From Figures 9a and 9d, we can see that TL2 connected the positive polarity in AR 8614 and the negative polarity to the west of AR 8626. At 06:21 UT, TL2 appears to have a cusp shape. More than an hour later, at 07:41 UT, in Figure 9e, it shows TL2 moves a little towards the west, and became a little faint (the continuous blue line marks the TL at 07:41 UT, the dotted blue line marks the previous TL at 06:21 UT). At 18:56 UT, TL2 on the right

became even fainter, but we can still identify the shape. On the left side, another faint TL appeared which connected the negative polarity in the northern hemisphere and positive in the southern hemisphere. The two TLs have a shape similar to field lines passing on both sides of an X point (where the magnetic field vanishes) in Figure 9c.

AR 8626 is a new-born active region, the coronal loops connecting the positive and negative polarity in this AR became increasingly larger. The distance between PMGC and NMGC of AR 8626 grew from the beginning of July 7 to the end of July 8 (Figure 5). The coronal loops in this AR extended northward.

Before the formation of TL2, the southern AR enlarged, with the distance between PMGC and NMGC becoming longer. The coronal loops grew in height as well, so the coronal loop in AR 8626 and in AR 8614 became closer, and they had eventually the possibility to be reconnected. As a result of magnetic reconnection, TL2 appeared with a cusp shape (Figure 9a). Another faint X-shape TL was also observed on the eastern side in Figure 9c.

4. Summary of Observations and Analysis

The formation and evolution of two homologous TLs are observed during July 6 to 8, in 1999, which connect AR 8614 from the northern hemisphere to AR 8626 in the southern hemisphere.

Before and during the formation period of the two TLs, both the distance between photospheric polarities and the height of coronal loops increased. These facts are confirmed by calculating the distances between PMGC and NMGC in both active regions quantitatively, and also demonstrated in the observations (Figures 7 and 9.)

Before the appearance of TL1, at early July 6, there is a dark region (Figure 7a) with similar shape of TL1 (Figure 7d). 11 hours later, there is nearly simultaneous appearance of TL1 all along its length (Figure 7d). These are indications that plasma density was already present in the corona before TL1 appearance. From Figure 8, the normalized intensity of TL1 has a sudden increase from 10:46 to 12:41 on July 7. From this phenomenon, we can deduce that the appearance of TL1 may be due to evaporation from the chromosphere. If we assume TL1 is a semi-circle above the solar surface, the length of TL1 is ~ 650 Mm. In the chromospheric evaporation process, the heated plasma typically expands with a velocity of $150 \sim 400$ km s^{-1} (Aschwanden, 2009; Doschek, 1990; Zhang *et al.*, 2016), where large flares involve a much higher input of energy and small flares involve lower input of energy. The energy release in TLs is much closer to that of the smallest flares. Here, the average plasma velocity in the TLs is assumed to be 150 km s^{-1}, which is similar to the velocities found in the smallest flares. In this scenario, the chromospheric evaporation has to fill the TL up to its middle, so we take half of the length. Therefore, a typical time needed to fill these loops would be about 36 minutes. During the period from 10:46 UT to 12:41 UT, in about 40 minutes, plasma filled TL1 through chromospheric evaporation.

The temperature varies at the same location before and after the TL1 appearance. A rough estimation of the temperature was 0.25 MK at the location of TL before its appearance, and it is 3.35 MK after its appearance. The temperatures of TL2 during different phases are also estimated, but due to the error inherent in temperature estimates using the filter-ratio method, the temperatures have not shown obvious change.

The formation and evolution process of TL1 (Figure 7) is observed on July 7. More than ten hours later, after the peak of TL1, TL2 appeared. Compared with TL2, TL1 is brighter, more extended, its southern end connected to a larger region of AR 8626 from east to west. Different from TL1, TL2 is narrower. Originally, a cusp shape appeared on the

right side, more than 10 hours later, another TL appeared on the left side (Figure 9c). For clarity, the TL on the right side of TL2 is named TL2R; the one on the left side is named TL2L.

The morphologies of TL1 and TL2R are similar to some extent, with some differences. The northern ends of the two originated from the same region, the positive magnetic polarity region in AR 8614. The location of the southern end of TL2R is almost the same as the end of the west edge of TL1. The shapes between TL1 and TL2R have little difference, TL2R has a cusp shape, and TL1 has a smoother emission distribution. When we compare Figure 7 and Figure 9, it is seen that a new bipolar region emerged to the right of TL2R, which made the shape of the TL become more curved. To the left of TL1, no TL appeared. For TL2, there is another TL on the left side (Figure 9c) which connect the negative magnetic polarity in the northern hemisphere to the positive magnetic polarity in the southern hemisphere. TL2R only appeared as a narrower loop at the west edge of TL1. That is likely related to the expansion of AR 8626 which is reconnecting more with its western bipolar region with time, so forming larger connections (the long connections of the quadrupole field), then later on the TL connection of AR 8614 is achieved with the leading negative polarity region in front of AR 8626, so the shape/extent of TL2 has differences with TL1.
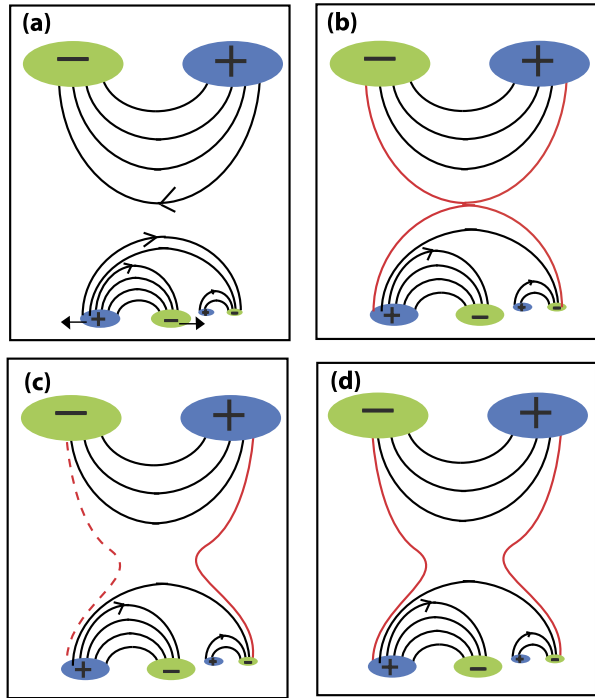
5. Discussion and Conclusions

Based on the presented observational results, TL1 and TL2 are likely created by the same mechanism. The large-scale transequatorial loops resulted from the expansion of the coronal loops of the two active regions. The antiparallel magnetic field configuration in the two active regions make magnetic reconnection possible. The energy released by the magnetic reconnection could heat the chromosphere, and cause chromospheric evaporation. As a result, soft X-rays are emitted by the hot plasma which fill the TL in a short period. Figure 8 shows that large amount of plasma fill the TL from both ends almost simultaneously. With the expansion of the coronal loops in the two hemispheres, when magnetic reconnection occurred, and X-shaped structure became observable, as seen in Figure 9c.

The likely formation mechanism for both TL1 and TL2 is depicted in Figure 10. The initial magnetic structures of AR 8614/8626 in the northern/southern hemisphere are shown, respectively, in Figure 10a. Following the increasing distance of the main photospheric polarities (Figures 3c and 5c), the coronal configuration of both ARs increased in volume, as outlined by the observed coronal loops. This is expected to induce magnetic reconnection between the two expanding magnetic configurations. This process is visualized in Figure 10b. After the magnetic reconnection, the two ARs became linked by two sets of field lines. A priory, a similar amount of energy is expected in both sets. However, in the first event, TL1 is only observed on the western side (continuous red line in panel c). The absence of a TL on the other side (dashed red line) is likely the consequence of not enough plasma present there, or not in the right range of the temperature. Several hours later, TL2 appeared (panel d). In this case, a faint TL is also present on the eastern side at the end of the observations (see attached movie).

The accumulated magnetic helicity in AR 8614 is negative (Figure 6a) from July 4 to 9 in 1999. The accumulated value of magnetic helicity in AR 8626 remains positive (Figure 6b) from July 7 to 9. A TL can connect ARs of opposite magnetic helicities. Indeed, during the reconnection process, the local helicities of reconnecting flux tubes will partly cancel in the reconnected flux tubes (keeping the total helicity conserved).

Figure 10 Schematic visualization of the topology and magnetic reconnection relevant to TL formation. (a) The initial magnetic structure of AR 8614/8626 in the northern/southern hemisphere, respectively. The two black filled arrows in the bottom show the two magnetic polarity regions separating from each other. (b) Magnetic reconnection between two loops of the different active regions. (c) The appearance of TL1. (d) The appearance of TL2.

Disclosure of Potential Conflicts of Interest   The authors declare that they have no conflicts of interest.

Publisher's Note   Springer Nature remains neutral with regard to jurisdictional claims in published maps and institutional affiliations.

References

Aschwanden, M.: 2009, *Physics of the Solar Corona*, Springer, Berlin 691.
Balasubramaniam, K.S., Pevtsov, A.A., Cliver, E.W., Martin, S.F., Panasenco, O.: 2011, *Astrophys. J.* **743**, 202.
Bao, S., Zhang, H.: 1998, *Astrophys. J.* **496**, L43.
Berger, M.A.: 1999, *Plasma Phys. Control. Fusion* **41**, B167.
Canfield, R.C., Hudson, H.S., McKenzie, D.E.: 1999, *Geophys. Res. Lett.* **26**, 627.
Chen, J., Bao, S., Zhang, H.: 2006, *Solar Phys.* **235**, 281. DOI.
Chen, J., Bao, S., Zhang, H.: 2007, *Solar Phys.* **242**, 65. DOI.

Chen, J., Lundstedt, H., Zhang, H.: 2010, *Adv. Space Res.* **45**, 537.

Chen, J., Lundstedt, H., Deng, Y., Wintoft, P., Zhang, Y.: 2011, *Solar Phys.* **273**, 51. DOI.

Démoulin, P., Berger, M.A.: 2003, *Solar Phys.* **215**, 203. DOI.

Doschek, G.A.: 1990, *Astrophys. J. Suppl.* **73**, 117.

Du, G.H., Chen, Y., Zhu, C.M., Liu, C., Ge, L.L., *et al.*: 2018, *Astrophys. J.* **860**, 40.

Fárník, M., Karlicky, M., Svestka, Z.: 1999, *Solar Phys.* **187**, 33. DOI.

Hao, J., Zhang, M.: 2011, *Astrophys. J. Lett.* **733**, 27L.

Khan, J., Hudson, H.: 2000, *Geophys. Res. Lett.* **27**, 1083.

Liu, J., Zhang, H.: 2006, *Solar Phys.* **234**, 21. DOI.

Luoni, M.L., Démoulin, P., Mandrini, C.H., van Driel-Gesztelyi, L.: 2011, *Solar Phys.* **270**, 45. DOI.

Moon, Y.J., Choe, G.S., Park, Y.D., Wang, H., Gallagher, P.T., Chae, J., Yun, H.S., Goode, P.R.: 2002, *Astrophys. J.* **574**, 434.

Pevtsov, A.: 2000, *Astrophys. J.* **531**, 553.

Pevtsov, A.A.: 2004, Transequatorial connections: Loops or magnetic separators? In: Stepanov, A.V., Benevolenskaya, E.E., Kosovichev, A.G. (eds.) *Multi-Wavelength Investigations of Solar Activity*, *Proceedings of IAU Symposium* **223**, Cambridge University Press, Cambridge, 521.

Pevtsov, A., Canfield, R.C., Metcalf, T.R.: 1994, *Astrophys. J.* **425**, L117.

Pevtsov, A., Canfield, R.C., Metcalf, T.R.: 1995, *Astrophys. J.* **440**, L109.

Poisson, M., Démoulin, P., López Fuentes, M., Mandrini, C.H.: 2016, *Solar Phys.* **291**, 1625. DOI.

Rust, D.M., Kumar, A.: 1996, *Astrophys. J.* **464**, L199.

Scherrer, P.H., Bogart, R.S., Bush, R.I., Hoeksema, J.T., Kosovichev, A.G., Schou, J.: 1995, *Solar Phys.* **162**, 129. DOI.

Švestka, Z., Krieger, A.S., Chase, R.C., Howard, R.: 1977, *Solar Phys.* **52**, 69. DOI.

Tsuneta, S.: 1991, *Solar Phys.* **136**, 37. DOI.

Tsuneta, S.: 1996, *Astrophys. J.* **456**, L63.

Wang, J.X., Zhang, Y.Z., Zhou, G.P., Harra, L.K., Williams, D.R., Jiang, Y.C.: 2007, *Solar Phys.* **244**, 75. DOI.

Xu, H., Gao, Y., Popova, E.P., Nefedov, S.N., Zhang, H., Sokoloff, D.D.: 2009, *Astron. Rep.* **53**, 160.

Yang, S., Büchner, J., Zhang, H.: 2009, *Astrophys. J.* **695**, L25.

Yokoyama, M., Masuda, S.: 2009, *Solar Phys.* **254**, 285. DOI.

Yokoyama, M., Masuda, S.: 2010, *Solar Phys.* **263**, 135. DOI.

Zhang, Y., Wang, J., Attrill, G.D.R., Harra, L.K., Yang, Z., He, X.: 2007, *Solar Phys.* **241**, 329. DOI.

Zhang, Q.M., *et al.*: 2016, *Astrophys. J.* **827**, 27.

Zhou, G., Wang, J., Zhang, J.: 2006, *Astron. Astrophys.* **445**, 1133.